Nonlinear counterion screening in colloidal suspensions

Hartmut Löwen,[a] Jean-Pierre Hansen, and Paul A. Madden[b]
Laboratoire de Physique, Ecole Normale Supérieure de Lyon, 69364 Lyon Cedex 07, France

A new "*ab initio*" method is presented which is designed to simulate highly asymmetric systems of charged particles such as micellar solutions and charge-stabilized colloidal suspensions. The hybrid description considers the macroion degrees of freedom explicitly, while the microscopic counterions are treated within the framework of density functional theory. The counterion density profile is treated as a dynamical variable which is coupled to the macroion positions; the corresponding equation of motions are derived from a Lagrangian which contains a fictitious kinetic energy term associated with the inhomogeneous counterion density, with a fictitious mass chosen so that the counterions stay as close as possible to the surface of lowest free energy (adiabatic condition). The discontinuous behavior of the counterion density profile at the macroion surfaces is suppressed by the use of a classical pseudopotential scheme without spoiling the rapid variation of the counterion density profile outside the macroion cores. The *ab initio* method is implemented in Molecular and Brownian Dynamics simulations of concentrated colloidal suspensions, and the results are compared to the predictions of much simpler simulations based on the pairwise additive effective Derjaguin–Landau–Verwey–Overbeek (DLVO) potential between macroions. The density profiles calculated from the DLVO model differ considerably from the predictions of the *ab initio* simulations, but the macroion pair structures are in reasonable agreement. Recent "improvements" of the standard DLVO theory are found to overestimate or underestimate the pair structure considerably. The density functional formalism may be used to derive systematic many-body corrections to the effective DLVO pair potential. The extension of the *ab initio* method to treat colloidal suspensions in the presence of added salt is briefly sketched.

I. INTRODUCTION

Charge-stabilized colloidal suspensions represent a severe challenge to a statistical mechanics description of their structure and dynamics due to the large asymmetry in size, mass, and charge between the mesoscopic polyions (or macroions) and the microscopic coions and counterions, not to speak of the molecules making up the suspending polar liquid (or "solvent"). The latter is almost invariably treated as a continuum, which is characterized by a macroscopic dielectric constant ϵ, reducing the electrostatic forces between ions, and which induces hydrodynamic interactions between the moving colloidal particles. These velocity-dependent forces do not affect the static equilibrium properties of the suspension, so that in the "primitive model" of colloidal suspensions, the dielectric constant ϵ is the only manifestation of the solvent. This reduction of the initial problem appears to be reasonable as long as the size of the solvent molecules is small compared to that of the macroions and to the Debye screening length of the microscopic ions.

The highly asymmetric primitive model has been the object of intense theoretical investigation for nearly 50 years. A further reduction of the initial many-component system may be achieved by taking advantage of the large asymmetry to eliminate the degrees of freedom of the microscopic ions, and derive effective interactions between "dressed" macroions, within the framework of the adiabatic approximation. This program may be carried out explicitly in the limit of low macroion concentration, where it leads to the pairwise additive screened Coulomb interaction between the electric double layers associated with the dressed macroions derived by Derjaguin *et al.* (DLVO potential).[1] This potential, which also includes the long-range van der Waals interactions between colloidal particles, has been widely used in theoretical calculations of the pair structure and of the phase diagram of charge-stabilized colloidal suspensions,[2] and in the interpretation of light and neutron scattering data of such dispersions, or of charged micellar solutions;[3] the surface charge carried by the macroion is often used to fit the experimental data to theoretical calculations of the structure factor based on the DLVO potential.

More recently, several attempts have been made to treat macroions and microscopic ions in the primitive model on an equal footing, using the multicomponent versions of the integral equations for the pair structure familiar from the theory of liquids,[4] or resorting to Monte Carlo (MC) or molecular dynamics (MD) computer simulations.[5] If the microscopic ions are assumed to be point ions and the "mean spherical" approximation (MSA) closure is used for the latter, the primitive model may again be reduced to a one-component problem with effective (screened) interactions between the dressed macroions. In

[a]Present address: Sektion Physik der Universität München, Theresienstrasse 37, D 8000 München 2, Germany.
[b]Permanent address: Physical Chemistry Laboratory, Oxford University, South Parks Road, Oxford OX1 3QZ, United Kingdom.

the low-concentration (Debye–Hückel) limit, the DLVO potential is recovered,[6] while at higher concentration, the effective macroion charge must be renormalized with respect to its Debye–Hückel value.[7–9]

Analytic reduction to pairwise additive effective potentials is only possible, for point coions and counterions, within the MSA. If more accurate closures such as the HNC equation are used, the resulting coupled integral equations must be solved numerically to obtain partial pair distribution functions. In practice, numerical solutions have only been obtained for moderate macroion charges (Z less than 100), typical of micellar solutions.[8,10] [An exception is the hybrid hypernetted chain (HNC)-MSA theory of Ref. 9, where higher charge asymmetries could be addressed.] A similar restriction holds for computer simulations; a recent, extensive MD study was carried out for a charge asymmetry 20:1 (Ref. 11), but it seems unlikely that significantly higher charge and size ratios may be tackled successfully in the near future.

In this paper, we present an alternative to "brute force" simulations by combining MD for the macroions with a density functional description of the microscopic ions. Rather than treating the degrees of freedom of the latter explicitly, we consider the inhomogeneous one-particle densities associated with each species in the instantaneous field of the macroions. Due to the large mass ratio, these densities follow adiabatically the motions of the macroions, and the forces acting between the latter are, in turn, determined by the inhomogeneous coion and counterion densities. In practice, a Lagrangian is used which couples the macroion degrees of freedom and the suitably parametrized densities; the resulting equations of motion yield the physical dynamics of the macroions, while an adequate choice of the fictitious mass associated with the densities ensures that the microscopic ions remain very near the surface of lowest free energy. Although the full implementation of this density functional strategy automatically accounts for nonlinear screening and more-than-two-body interactions between macroions, it will be shown to lead back to the effective DLVO potential under well-defined conditions and to allow the derivation of systematic corrections to the approximation of pairwise additivity.

The method presented in this paper may be looked upon as a purely classical counterpart of the *ab initio* method developed by Car and Parrinello[12] to treat valence electron states in covalent or metallic materials,[13] the coions and counterions, which obey classical statistical mechanics, here playing the role of the degenerate valence electrons. In fact, large parts of a Car–Parrinello code may be carried over to construct the density functional code for colloidal suspensions. A preliminary account of parts of the present work has been published elsewhere.[14]

II. THE PRIMITIVE MODEL OF CHARGE-STABILIZED COLLOIDS

The basic model under consideration here is an extension of the familiar primitive model of ionic solutions to *highly* asymmetric suspensions of ionized spherical colloidal particles in a polar liquid. As emphasized earlier, the

molecular nature of the latter is ignored and it manifests itself solely through its macroscopic properties—the dielectric constant ϵ as far as static properties of the primitive model are concerned, and the viscosity η_s which determines the friction coefficient $\xi = 6\pi\eta_s R$ if dynamical properties are to be examined.

For clarity and convenience, we shall first restrict ourselves to perfectly dialyzed suspensions, i.e., the concentration of added salt will be assumed to vanish; the generalization to the case where this concentration is finite will be examined in Sec. X. Under these conditions, the model is made up of two ionic species—the macroions of radius R, mass M, and charge Ze; and the counterions of radius r, mass m, and charge $-qe$, and we are interested in situations where $R/r \gg 1$, $M/m \gg 1$, and $Z/q \gg 1$. Because the Coulomb repulsion keeps the counterions apart, and since $r \ll R$, it is a reasonable approximation to neglect their size, i.e., to assume $r = 0$ (point counterions). In the absence of added salt, the Debye screening length and hence the width of the electric double layers around the macroions is generally comparable to their size, so that the van der Waals interactions are masked effectively by the Coulomb interactions and may hence be safely neglected. Under these conditions, the primitive model pair potentials read

$$v_{mm}(r) = \begin{cases} \infty, & \text{for} \quad r \leqslant 2R \\ \dfrac{Z^2 e^2}{\epsilon r}, & \text{for} \quad r > 2R, \end{cases} \tag{1}$$

$$v_{mc}(r) = \begin{cases} \infty, & \text{for} \quad r \leqslant R \\ -\dfrac{Zqe^2}{\epsilon r}, & \text{for} \quad r > R, \end{cases} \tag{2}$$

$$v_{cc}(r) = \dfrac{q^2 e^2}{\epsilon r}, \tag{3}$$

where the indices m and c are for macroions and counterions, respectively. If n_m and n_c are the numbers of macroions and counterions per unit volume, global charge neutrality requires that

$$Zn_m = qn_c. \tag{4}$$

For given values of Z, q, R, and ϵ, the equilibrium properties of the suspension depend on the temperature T and the number density n_m, n_c being determined by the constraint (4). It is convenient to introduce the dimensionless variables $\eta = 4\pi n_m R^3/3$ (packing fraction of the macroions) and $\Gamma = q^2 l/a_c$, where $l = e^2/\epsilon k_B T$ is the Bjerrum length ($l = 7.2$ Å in water at room temperature) and $a_c = (3/4\pi n_c)^{1/3}$ is the ion-sphere radius of the counterions. The parameter Γ is a direct measure of the intensity of Coulomb coupling between counterions. The other important length in the problem is the Debye screening length associated with the counterions

$$\lambda_D = \frac{1}{\kappa_D} = \sqrt{\frac{\epsilon k_B T}{4\pi n_c q^2 e^2}}. \tag{5}$$

One of two strategies may now be followed in order to arrive at the main objective of a statistical theory of the

colloidal suspension, namely, the measurable properties of the mesoscopic fluid of colloidal particles such as the macroion pair structure,[2,3] or the phase diagram.[15]

The first strategy treats both ionic species on an equal footing by focusing on the three partial pair distribution functions $g_{mm}(r)$, $g_{mc}(r)$, and $g_{cc}(r)$. These may be calculated either "exactly" from MC or MD simulations,[11] or approximately from numerical solutions of coupled integral equations such as HNC, MSA, or hybrid closures.[8–11,16] This strategy has a drawback. For technical reasons, the simulations and the numerical solutions of the more accurate integral equations are limited to size and charge asymmetries that fall into the range of micellar solutions rather than colloidal suspensions. As already mentioned earlier, the counterion component may be formally eliminated if their correlations and the macroionic correlations are treated within the linear MSA closure.[6,8,9] The resulting effective pair potential between macroions is of the DLVO form

$$v_{mm}^{\mathrm{eff}}(r) = \frac{Z_{\mathrm{eff}}^2 \exp(-\kappa_D r)}{\epsilon r}, \quad r > \sigma \equiv 2R. \qquad (6)$$

In the low concentration (or Debye–Hückel) limit, the DLVO expression for Z_{eff} is recovered,[6] namely

$$Z_{\mathrm{eff}}^{\mathrm{DLVO}} = \frac{Z \exp(\kappa_D R)}{1 + \kappa_D R}. \qquad (7)$$

Note that at higher concentrations, Z_{eff} is enhanced above its DLVO limit (7).[8,9] The effective pair potential (6) may then be used in a one-component description of the colloidal suspension to calculate $g_{mm}(r)$.

The approach based on the MSA has several shortcomings. The pairwise additivity can be seen to be a direct consequence of the linear character of the MSA closure which, for point counterions, breaks down as the concentration increases. The simplicity of the derivation of an effective pair potential between macroions is spoiled, as soon as finite size effects are included,[8,9] which is a necessity in the presence of added salt due to the Coulomb collapse of oppositely charged point ions. In fact, the effective macroion charge Z_{eff} in Eq. (6) is frequently used as an adjustable parameter in an analysis of experimental scattering data.[3]

The alternative strategy, which will be pursued here, focusses on the inhomogeneous one-particle density $\rho_c(\mathbf{r})$ of the counterions. Historically, the first attempt along these lines is the familiar Poisson–Boltzmann theory, which, in its linearized version, has led to the DLVO potential between macroions.[1] At high concentrations, when the macroion structure exhibits strong short-range or even crystalline order, the Poisson–Boltzmann equation may be solved in a Wigner–Seitz cell to determine $\rho_c(\mathbf{r})$ around a single macroion. Such solutions have been used to determine effective macroion charges in a DLVO potential.[17] Poisson–Boltzmann theory may be generalized to incorporate correlation effects and to treat multicenter macroion geometries within the framework of the density functional theory of inhomogeneous liquids.[18,19] The density-

functional formulation will be presented in Sec. III, while practical implementations will be the subject of the remaining sections of this paper.

III. A DENSITY-FUNCTIONAL FORMULATION

If the macroion and counterion coordinates and momenta are denoted by $\{\mathbf{R}_i, \mathbf{P}_i\}$ ($1 \leqslant i \leqslant N_m$) and $\{\mathbf{r}_j, \mathbf{p}_j\}$ ($1 \leqslant j \leqslant N_c$), respectively, the total primitive model Hamiltonian reads

$$H = K_m[\{\mathbf{P}_i\}] + K_c[\{\mathbf{p}_i\}] + V_{mm}[\{\mathbf{R}_i\}]$$
$$+ V_{mc}[\{\mathbf{R}_i\}, \{\mathbf{r}_j\}] + V_{cc}[\{\mathbf{r}_j\}], \qquad (8)$$

where K_m and K_c are the kinetic energies, while V_{mm}, V_{mc}, and V_{cc} are the potential energies, sums over all pairs of the interactions (1)–(3). Since $M/m \gg 1$, the time scales τ_m and τ_c associated with the two species differ by several orders of magnitude, so that partial averaging over the degrees of freedom may be carried out for a given configuration $\{\mathbf{R}_i\}$ of the macroions, which provide an "external" field in which the counterions move (adiabatic approximation). As shown in the Appendix, the effective Hamiltonian for the macroions reduces to

$$H = K_m[\{\mathbf{P}_i\}] + V_{mm}[\{\mathbf{R}_i\}] + \mathscr{F}[\rho_c(\mathbf{r})], \qquad (9)$$

where $\mathscr{F}$ is the free energy of the inhomogeneous counterion fluid, a *functional* of the one-particle density $\rho_c(\mathbf{r})$, which depends parametrically on the macroion positions $\{\mathbf{R}_j\}$.[20] This functional is the sum of four terms[19]

$$\mathscr{F} = \mathscr{F}_{\mathrm{id}} + \mathscr{F}_{\mathrm{ext}} + \mathscr{F}_{cc} + \mathscr{F}_{\mathrm{corr}}, \qquad (10)$$

$$\mathscr{F}_{\mathrm{id}} = k_B T \int d\mathbf{r} \, \rho_c(\mathbf{r}) \{ \ln[\Lambda_c^3 \rho_c(\mathbf{r})] - 1 \}, \qquad (11)$$

$$\mathscr{F}_{\mathrm{ext}} = \int d\mathbf{r} \, \rho_c(\mathbf{r}) V_{\mathrm{ext}}[r, \{\mathbf{R}_j\}]$$

$$= \sum_{j=1}^{N_m} \int d\mathbf{r} \, \rho_c(\mathbf{r}) v_{mc}(|\mathbf{r} - \mathbf{R}_j|), \qquad (12)$$

$$\mathscr{F}_{cc} = \frac{q^2 e^2}{2\epsilon} \iint d\mathbf{r} \, d\mathbf{r}' \frac{\rho_c(\mathbf{r}) \rho_c(\mathbf{r}')}{|\mathbf{r} - \mathbf{r}'|}. \qquad (13)$$

In the "ideal" part (11), Λ_c is the de Broglie thermal wavelength of the counterions, $\mathscr{F}_{\mathrm{ext}}$ describes the coupling of the latter to the macroions, while $\mathscr{F}_{cc}$ stems from the Coulomb interaction between counterions (the precise status of this term is discussed in the Appendix). The last term in Eq. (10) is the nontrivial counterion correlation term, for which we adopt the local density approximation (LDA)

$$\mathscr{F}_{\mathrm{corr}} = k_B T \int d\mathbf{r} \, \rho_c(\mathbf{r}) \Psi_{\mathrm{OCP}}^{\mathrm{exc}}[T, \rho_c(\mathbf{r})]. \qquad (14)$$

In Eq. (14), $\Psi_{\mathrm{OCP}}^{\mathrm{exc}}$ denotes the reduced excess free energy per ion $F^{\mathrm{exc}}/N k_B T$ of a homogeneous fluid of point ions in neutralizing, uniform background (the so-called "one-component plasma" or OCP[21]). Due to the scaling properties of the Coulomb potential, $\Psi_{\mathrm{OCP}}^{\mathrm{exc}}$ depends only on the dimensionless coupling constant Γ defined in Sec. II. The

function $f(\Gamma)=\Psi_{OCP}^{exc}[T,\rho_c(\mathbf{r})]$ is well known, from diagrammatic expansions at low Γ, and from extensive MC simulations at large Γ.[21] In practice, under physical conditions relevant for concentrated colloidal suspensions, Γ remains less than 1, so that $f(\Gamma)$ is given, to a high degree of accuracy, by the Abe expansion[22]

$$\Psi_{OCP}^{exc}(T,\rho_c)=-\frac{1}{\sqrt{3}}\Gamma^{3/2}-\frac{c}{3}\Gamma^3-\frac{1}{8}\Gamma^3(3\ln\Gamma-1)$$

$$+O(\Gamma^{9/2}), \qquad (15)$$

where $c=\frac{9}{8}\ln 3+\frac{3}{2}\gamma-1=1.101\,762\,3\cdots$, and γ is Euler's constant; note that the leading term in Eq. (15) is just the familiar Debye–Hückel contribution.

So far the only approximation that has been made is the LDA for $\mathscr{F}_{corr}$. This is justified as long as $\rho_c(\mathbf{r})$ varies smoothly in space; more precisely, $\rho_c(\mathbf{r})$ should vary little over a distance of the order of the mean spacing between counterions, i.e., $|\nabla\ln\rho_c(\mathbf{r})|<[\rho_c(\mathbf{r})]^{1/3}$. Under the weak screening conditions typical of salt-free suspensions, this condition is easily satisfied, except perhaps in the immediate vicinity of the macroion surfaces, where the counterions pile up due to the strong Coulomb attraction ("Stern layer"). Nonlocal corrections[18] to the LDA may then be necessary, but the difficulty will be overcome differently in the MD simulation described in Secs. VI–IX.

For each macroion configuration, the equilibrium one-particle density $\rho_c^{(0)}[\mathbf{r},\{\mathbf{R}_i\}]$ is the solution to the variational problem

$$\frac{\delta\mathscr{F}}{\delta\rho_c}\bigg|_{\rho_c=\rho_c^{(0)}(\mathbf{r})}=0 \qquad (16)$$

subject to the constraint of global charge neutrality

$$\int d\mathbf{r}\,\rho_c(\mathbf{r})=N_c=\frac{Z}{q}N_m. \qquad (17)$$

Once $\rho_c^{(0)}$ has been determined, the force induced by the counterions acting on each macroion may be calculated directly according to the Hellmann–Feynman theorem

$$\mathbf{F}_j^c=-\nabla_{\mathbf{R}_j}\mathscr{F}(\{\rho_c^{(0)}[\mathbf{r},\{\mathbf{R}_j\}]\};\{\mathbf{R}_j\})$$

$$=-\int d\mathbf{r}\,\rho_c[\mathbf{r},\{\mathbf{R}_j\}]\nabla_{\mathbf{R}_j}v_{mc}(|\mathbf{r}-\mathbf{R}_j|) \qquad (18)$$

for $1\leqslant j\leqslant N_m$. Note that in order to obtain the total force acting on macroion j, one must add the pairwise additive contribution due to the direct Coulomb interaction between macroions (v_{mm}).

IV. DERIVATION OF THE DLVO POTENTIAL

Solution of the general variational problem sketched above presents a formidable mathematical challenge due to the nonlinear nature of the resulting Euler equation. Before describing the numerical scheme which we have developed to solve the problem, it is important to show which further approximations have to be made within the present density-functional formulation in order to recover the standard DLVO description, which is essentially a linearized

theory. $\mathscr{F}_{ext}$ and $\mathscr{F}_{cc}$ in Eqs. (10)–(14) are linear and quadratic functionals of $\rho_c(\mathbf{r})$ which yield constant and linear terms in the Euler equation. $\mathscr{F}_{id}$ and $\mathscr{F}_{corr}$, on the other hand, may be expanded to quadratic order around the mean counterion density $\overline{\rho_c}=n_c$, a valid procedure for weak inhomogeneities

$$\mathscr{F}_{id}+\mathscr{F}_{corr}\simeq\mathscr{F}_q=F_0+\int d\mathbf{r}\bigg\{B[\rho_c(\mathbf{r})-\overline{\rho_c}]$$

$$+\frac{A}{2}[\rho_c(\mathbf{r})-\overline{\rho_c}]^2\bigg\}. \qquad (19)$$

The coefficients B and A may be calculated explicitly from Eqs. (11) and (14) using the Abe expansion (15) with the result

$$B=k_BT\bigg\{\ln(\Lambda^3\overline{\rho_c})-\frac{\sqrt{4\pi\overline{\rho_c}}}{2}q^3l^{3/2}+\frac{8\pi\overline{\rho_c}}{3}\bigg(\frac{1}{16}-\frac{c}{3}\bigg)q^6l^3$$

$$-\pi q^6l^3\overline{\rho_c}\ln\bigg[q^2l\bigg(\frac{4\pi\overline{\rho_c}}{3}\bigg)^{1/3}\bigg]\bigg\}, \qquad (20)$$

$$A=k_BT\bigg\{\frac{1}{\overline{\rho_c}}-\frac{1}{4}\bigg(\frac{4\pi}{\overline{\rho_c}}\bigg)^{1/2}q^3l^{3/2}-\frac{8\pi}{3}\bigg(\frac{1}{16}+\frac{c}{3}\bigg)q^6l^3$$

$$-\pi q^6l^3\overline{\rho_c}\ln\bigg[q^2l\bigg(\frac{4\pi\overline{\rho_c}}{3}\bigg)^{1/3}\bigg]\bigg\}, \qquad (21)$$

where l is the Bjerrum length defined in Sec. II.

For illustrative purposes, consider first the case of point macroions ($R=0$). Since the potentials $v_{mc}(r)$ and $v_{cc}(r)$ are then integrable, the equilibrium density $\rho_c^0[\mathbf{r},\{\mathbf{R}_i\}]$ may be obtained analytically from Eq. (16) by Fourier transformation. The solution is a linear superposition of screened Coulomb (or Yukawa) orbitals

$$\rho_c^{(0)}[\mathbf{r},\{\mathbf{R}_i\}]=\sum_{i=1}^{N}\frac{Z}{q}\frac{\kappa^2}{4\pi}\frac{\exp(-\kappa|\mathbf{r}-\mathbf{R}_i|)}{|\mathbf{r}-\mathbf{R}_i|}, \qquad (22)$$

where

$$\kappa^2=\frac{4\pi q^2 e^2}{\epsilon A}. \qquad (23)$$

If the contribution from $\mathscr{F}_{corr}$ to $\mathscr{F}_q$ is neglected, $A=k_BT/\overline{\rho_c}$, and κ reduces to the Debye–Hückel expression κ_D [Eq. (5)]. Inserting the result (22) into the Hellmann–Feynman expression (18), one recovers an effective macroion–macroion pair potential:

$$v_{mm}^{eff}(r)=\frac{Z^2e^2}{\epsilon r}\exp(-\kappa r), \qquad (24)$$

which is the DLVO potential (6) for $R=0$. Note that counterion correlations renormalize κ with respect to its DLVO value κ_D, but the correction is generally negligible, at least in the salt-free case under consideration here.

A finite macroion radius R forces $\rho_c^{(0)}[\mathbf{r},\{\mathbf{R}_i\}]=0$ for $|\mathbf{r}-\mathbf{R}_i|<R$. The finite R correction to the potential (24) is obtained most conveniently by adopting for $\rho_c^{(0)}$ the linear superposition form (22), and imposing the following

constraint on the one-particle density around a macroion situated at the origin:

$$\int_{|\mathbf{r}|>R} d\mathbf{r}\, \rho_c(\mathbf{r}) = \frac{Z}{q} . \tag{25}$$

This constraint is incorporated into the free energy functional by a Lagrange multiplier $\tilde{\mu}$. Determination of $\tilde{\mu}$ finally leads to the renormalized charge given by Eq. (7) (with κ replacing κ_D); the equilibrium density ρ_c^{DLVO} is given by Eq. (22), for $|\mathbf{r}-\mathbf{R}_i|>R$, and Z replaced by $Z_{\text{eff}}^{\text{DLVO}}$,

$$\rho_c^{\text{DLVO}}[\mathbf{r},\{\mathbf{R}_i\}] = \sum_{i=1}^{N} \frac{Z_{\text{eff}}^{\text{DLVO}}}{q} \frac{\kappa^2}{4\pi} \frac{\exp(-\kappa|\mathbf{r}-\mathbf{R}_i|)}{|\mathbf{r}-\mathbf{R}_i|},$$
$$|\mathbf{r}-\mathbf{R}_i|>R. \tag{26}$$

The enhancement of the macroion charge from Z to $Z_{\text{eff}}^{\text{DLVO}}$ is a direct consequence of the core condition (25) which expresses that the counterion charge *outside* the macroion core must exactly cancel the bare charge Z of the latter. The resulting effective macroion–macroion pair potential takes the DLVO form (6).

Note that throughout the treatment of the finite size of the macroions, the overlap of Yukawa orbitals associated with different macroions has been neglected implicitly, so that the result only applies to dilute suspensions.

The above considerations show that the DLVO potential is contained as a special limiting case in the general density functional formulation of the preceding section, and also give some hints of how to go beyond the DLVO theory. The above derivation clearly establishes a link between pairwise additivity of the effective forces between macroions and the quadratic nature of the approximate free energy functional (19). Terms beyond quadratic in the expansion of $\mathscr{F}_{\text{id}} + \mathscr{F}_{\text{corr}}$ would lead to more-than-two-body effective forces between macroions, so that the DLVO theory can, in principle, be improved systematically by adding these many-body forces, as shown in the following section.

V. MANY-BODY FORCES BETWEEN MACROIONS

The density functional framework will now be used in a systematic perturbation scheme to derive formal expressions for effective many-body interactions between "dressed" macroions. The reference free energy functional $\mathscr{F}_0$ is chosen to be Eq. (10), with $\mathscr{F}_{\text{id}} + \mathscr{F}_{\text{corr}}$ replaced by their quadratic form (19)

$$\mathscr{F}_0 = \mathscr{F}_q + \mathscr{F}_{\text{ext}} + \mathscr{F}_{cc}, \tag{27}$$

while the perturbation is

$$\lambda \mathscr{F}' = \mathscr{F}_{\text{id}} + \mathscr{F}_{\text{corr}} - \mathscr{F}_q, \tag{28}$$

where λ is an ordering parameter to be set equal to 1 at the end of the calculation. The equilibrium density which minimizes $\mathscr{F}_0$ is the DLVO density $\rho_c^{\text{DLVO}}(\mathbf{r}\{\mathbf{R}_i\})$ defined in Eq. (26), at least in the limit of low macroion concentrations. The density minimizing the full functional $\mathscr{F} = \mathscr{F}_0 + \lambda \mathscr{F}'$ is sought in the form of an expansion in powers of λ,

$$\rho_c^{(0)}[\mathbf{r},\{\mathbf{R}_i\}] = \rho_c^{\text{DLVO}}[\mathbf{r},\{\mathbf{R}_i\}] + \sum_{n=1}^{\infty} \lambda^n \rho_{cn}[\mathbf{r},\{\mathbf{R}_i\}]. \tag{29}$$

Substituting Eq. (29) into $\mathscr{F}$ and expanding $\delta\mathscr{F}/\delta\rho_c$ in powers of λ, one finds for the first-order term

$$\rho_{c1}[\mathbf{r},\{\mathbf{R}_i\}] = \hat{\rho}_1[\mathbf{r},\{\mathbf{R}_i\}] - \frac{\kappa^2}{4\pi} \int d\mathbf{r}' \frac{\exp(-\kappa|\mathbf{r}-\mathbf{r}'|)}{|\mathbf{r}-\mathbf{r}'|}$$
$$\times \hat{\rho}_1[\mathbf{r},\{\mathbf{R}_i\}], \tag{30}$$

where

$$\hat{\rho}_1[\mathbf{r},\{\mathbf{R}_i\}] = -\frac{1}{A} \left[\frac{\partial f \rho_c^{\text{DLVO}}[\mathbf{r},\{\mathbf{R}_i\}]}{\partial \rho} - B \right.$$
$$\left. -A[\rho_c^{\text{DLVO}}[\mathbf{r},\{\mathbf{R}_i\}] - \bar{\rho}_c] \right\} \tag{31}$$

and

$$f(\rho) = \rho[\ln(\Lambda_c^3 \rho) - 1 + \Psi_{\text{OCP}}^{\text{exc}}(T,\rho)]. \tag{32}$$

In first-order perturbation theory, one may now derive systematically effective many-body interactions between macroions by taking expansion (19) of $f(\rho)$ to orders higher than quadratic in $[\rho_c(\mathbf{r}) - \bar{\rho}_c]$. The sum of all more-than-two-body terms leads to a potential energy between macroions of the form

$$V_{\text{total}}[\{\mathbf{R}_i\}] = \sum_{n=3}^{\infty} V^{(n)}[\{\mathbf{R}_i\}] \tag{33}$$

with

$$V^{(n)}[\{\mathbf{R}_i\}] = \frac{1}{n!} \int d\mathbf{r}\, \frac{\partial^n f(\bar{\rho}_c)}{\partial \rho^n} [\rho_c^{\text{DLVO}}(\mathbf{r},\{\mathbf{R}_i\}) - \bar{\rho}_c]^n. \tag{34}$$

This general procedure may be taken to higher order in the perturbation expansion (29), but the expressions become very cumbersome for practical purposes. In the following sections, it will be shown how the minimization of the full functional may be implemented numerically to compute the instantaneous effective forces between dressed macroions in an MD code.

VI. DENSITY FUNCTIONAL AND MOLECULAR DYNAMICS

In order to solve the variational problem of Eqs. (16) and (17) self-consistently and adiabatically, along the macroion trajectories, we follow the ideas of Car and Parrinello[12,13] and regard the counterion density $\rho_c(\mathbf{r})$, or, equivalently, its Fourier components $\rho_{\mathbf{k}c}$ as dynamical variables coupled to the macroion degrees of freedom by the free energy functional $\mathscr{F}$. Classical equations of motion for $\rho_c(\mathbf{r})$ and the macroion degrees of freedom $\mathbf{R}_i$ are derived from the Lagrangian

$$\mathcal{L} = \frac{1}{2} M \sum_{j=1}^{N_m} \dot{\mathbf{R}}_j^2 + \frac{1}{2} m_f \int d\mathbf{r} [\dot{\rho}_c(\mathbf{r})]^2$$

$$- \sum_{i<j} v_{mm}(|\mathbf{R}_i - \mathbf{R}_j|) - \mathcal{F}([\rho_c(\mathbf{r})];\{\mathbf{R}_j\}). \quad (35)$$

In Eq. (35), m_f is a "fake" mass (in fact a mass times the fifth power of a length) associated with $\rho_c(\mathbf{r})$. If, in appropriate units, m_f is chosen much smaller than M, the resulting $\rho_c[\mathbf{r},\{\mathbf{R}_j\}]$ is expected to stay close to the true adiabatic $\rho_c^{(0)}[\mathbf{r},\{\mathbf{R}_j\}]$ which would follow, e.g., from a simulated annealing procedure for each macroion configuration $\{\mathbf{R}_j\}$.

The coupled equations of motion derived from the Lagrangian (35) are of the form

$$M\ddot{\mathbf{R}}_i = - \sum_{i \neq j} \nabla_i v_{mm}(|\mathbf{R}_i - \mathbf{R}_j|) + \mathbf{F}_i^c, \quad (36)$$

$$m_f \ddot{\rho}_c(\mathbf{r}) = - \frac{\delta \mathcal{F}}{\delta \rho_c(\mathbf{r})}$$

$$= - k_B T \ln[\Lambda_c^3 \rho_c(\mathbf{r})] - \phi_{mc}(\mathbf{r}) - \phi_{cc}(\mathbf{r})$$

$$- k_B T \chi_{\text{OCP}}^{\text{exc}}[T,\rho_c(\mathbf{r})]. \quad (37)$$

In Eq. (36), $\mathbf{F}_i^c$ is the force on macroion i induced by the counterions, and given by Eq. (18). In Eq. (37), ϕ_{mc} and ϕ_{cc} are the Coulomb potentials acting on a counterion at $\mathbf{r}$, and due to the macroions and other counterions,

$$\phi_{mc}(\mathbf{r}) = \sum_{i=1}^{N_m} v_{mc}(|\mathbf{r} - \mathbf{R}_i|) \quad (38)$$

$$\phi_{cc}(\mathbf{r}) = \frac{q^2 e^2}{\epsilon} \int d\mathbf{r}' \frac{\rho_c(\mathbf{r}')}{|\mathbf{r} - \mathbf{r}'|}, \quad (39)$$

while $\chi_{\text{OCP}}^{\text{exc}}(T,\rho_c) = \Psi_{\text{OCP}}^{\text{exc}}(T,\rho_c) + \rho_c \partial \Psi_{\text{OCP}}^{\text{exc}}/\partial \rho_c$.

In practice, $\rho_c(\mathbf{r})$ is parametrized by its expansion in Fourier components

$$\rho_c(\mathbf{r}) = \sum_{\mathbf{k}} \rho_{\mathbf{k}c} \exp(i\mathbf{k}\cdot\mathbf{r}), \quad (40)$$

where the sum is over all reciprocal lattice vectors $\mathbf{k}$ of the periodically repeated simulation box of volume V; conversely,

$$\rho_{\mathbf{k}c} = \frac{1}{V} \int_V d\mathbf{r}\, \rho_c(\mathbf{r})\exp(-i\mathbf{k}\cdot\mathbf{r}). \quad (41)$$

The resulting density in $\mathbf{r}$ space is defined on a cubic $\mathcal{N}^3$-dimensional grid. The finite difference versions of Eqs. (36) and (37) are solved iteratively by the standard Verlet algorithm,[4,5] and efficient fast Fourier transform (FFT) techniques are used to commute back and forth between the $\mathbf{r}$- and $\mathbf{k}$-space representations of the counterion density.[13] The infinite range of the bare Coulomb interactions is taken care of by appropriate Ewald summation.[5,23]

VII. A MACROION–COUNTERION PSEUDOPOTENTIAL

The *ab initio* combination of density functional theory and MD sketched in the previous section raises a technical

problem linked to the rapid variation of $\rho_c(\mathbf{r})$ in the vicinity of the macroion surfaces. Due to the combination of excluded volume effects for $|\mathbf{r} - \mathbf{R}_i| < R$ and strong Coulomb attraction for $|\mathbf{r} - \mathbf{R}_i| > R$, the counterions pile up in the "Stern-layer" part of the electric double layers, where $\rho_c(\mathbf{r})$ rises sharply above the mean counterion density $\bar{\rho}_c$. Hence a very large number of Fourier components $\rho_{\mathbf{k}c}$ would be required to yield a sufficiently accurate representation of $\rho_c(\mathbf{r})$.

To overcome this technical difficulty, we developed a pseudopotential scheme, similar to that used in the quantum-mechanical ion–electron problem, designed to suppress the discontinuous behavior of the local density $\rho_c(\mathbf{r},\{\mathbf{R}_i\})$ at the macroion surfaces. The present, purely classical procedure involves two closely related steps.

First, the macroion–counterion core repulsion is suppressed and the Coulomb attraction is smoothly extrapolated inside the macroion core, such that the true potential $v_{mc}(r)$ in Eq. (2) is replaced by the "pseudopotential"

$$v'_{mc}(r) = - \frac{Zqe^2}{\epsilon r} erf(r/R_c), \quad (42)$$

where R_c is chosen to be $\simeq R/2$. In other words, we allow the counterions to penetrate the macroion cores; this leads to an extra, unphysical, counterion charge inside the cores, which must be compensated by increasing the macroion charge from Ze to $(Z+Z^*)e$. Since the total macroion charge, i.e., the sum of the renormalized surface charge plus the counterion charge of opposite sign inside the core, must, on the average, remain equal to the physical charge Ze, the mean counterion density $\bar{\rho}_c$ has to be increased accordingly. It must be stressed that Z^* is *not* an adjustable parameter, but is uniquely determined as explained below.

However, it is clear that the permeability of the macroions leads to unwanted fluctuations of the counterion charge density inside the cores, and hence of the apparent macroion charge, which will strongly affect the static and dynamical properties of the macroion fluid. Therefore, in a second step of the pseudopotential construction, these fluctuations are efficiently damped by simultaneously assigning a severe free energy handicap to the excess counterion charge. This is achieved by modifying the free energy functional for counterion densities exceeding a cut-off value ρ_c^{cut}, so as to "stiffen" $\rho_c(\mathbf{r})$ inside the cores. In practice, we added an arbitrary, positive free energy contribution $f_{\text{cut}}(\rho_c)$ to $\Psi_{\text{OCP}}^{\text{exc}}(T,\rho)$ in Eq. (14), which increases rapidly for counterion densities $\rho_c > \rho_c^{\text{cut}}$; the form chosen for f_{cut} is

$$f_{\text{cut}}(\rho_c) = \begin{cases} 0, & \text{when } x \equiv (\rho_c - \rho_c^{\text{cut}})/\rho_c^{\text{cut}} < 0 \\ 0.05 \exp\left[-\dfrac{3}{\tan(\pi x)}\right], & \text{when } x \geqslant 0. \end{cases} \quad (43)$$

The whole pseudopotential procedure sketched above should result in a counterion density $\rho_c(\mathbf{r})$ which is smooth inside the macroion cores, but coincides with the physical density outside the cores. Under these conditions the construction is norm conserving.

The auxiliary parameters Z^* and ρ_c^{cut} have to be determined self-consistently, for each thermodynamic state, before the corresponding MD run. In fact, these parameters are expected to depend on any particular macroion configuration $\{\mathbf{R}_i\}$; their determination would hence require, in principle, a large number of exploratory runs for each typical macroion configuration, a highly unpractical procedure. However, it is reasonable to assume that the optimum parameters Z^* and ρ_c^{cut} are only weakly dependent on the configurations $\{\mathbf{R}_i\}$. Hence we have chosen one typical configuration, in a highly simplified geometry, to determine Z^* and ρ_c^{cut}, and checked *a posteriori* that these values lead to negligible fluctuations of the effective macroion charges, as the ionic configurations evolve during a MD simulation. The geometry chosen is that of a single macroion in its spherical Wigner–Seitz cell, containing a total counterion charge which exactly cancels the macroion charge.[17] This geometry is well adapted to highly symmetric crystal configurations, but is also representative of dense fluid configurations characterized by crystal-like short-range order.

The volume of the Wigner–Seitz cell centered on a macroion is equal to the volume per macroion $v_m = V/N_m = 1/n_m$. The counterion density $\rho_c(\mathbf{r})$ inside the cell has spherical symmetry and its integral over the volume v_m must equal Z/q; $\rho_c(\mathbf{r})$ is obtained numerically by solving the variational problem (16) with the simplified free energy functional (10), where the coupling to the macroions $\mathscr{F}_{ext}$ reduces to a single term, corresponding to the macroion at the center of the spherical Wigner–Seitz cell; the imposed boundary condition is $d\rho_c(r)/dr = 0$ on the surface of the Wigner–Seitz sphere, i.e., for $r = R_{WS} = (3v_m/4\pi)^{1/3}$. If, moreover, the correlation contribution (14) was neglected, the problem would reduce to the Poisson–Boltzmann problem considered by Alexander *et al.*[17] The parameters ρ_c^{cut} and Z^* were then determined for the Wigner–Seitz geometry as follows: $\rho_c(\mathbf{r})$ was first calculated outside the macroion core ($R < r < R_{WS}$), and ρ_c^{cut} was chosen equal to the value $\rho_c(r=R)$ at the surface of the impenetrable macroion. Next the penetrable ion version of the model, based on the pseudopotential (42), was solved after adding the contribution $f_{cut}(\rho_c)$ to the correlation part of the counterion free energy. Z^* was varied until the total (effective) charge of the penetrable macroion matched the physical charge Ze of the impenetrable macroion. In view of the spherical symmetry and of Gauss' theorem, these two counterion densities (corresponding to impenetrable and penetrable macroions, respectively) are exactly equal outside the cores. Whereas the former density has a discontinuity when $|\mathbf{r}-\mathbf{R}_i| = R$ and drops to zero inside the cores, the latter remains smooth throughout the Wigner–Seitz cell.

While it is clear that the two densities may differ for more general macroion configurations, we found that the parameters ρ_c^{cut} and Z^*, determined within the Wigner–Seitz geometry, are in fact transferrable. *A posteriori* tests, carried out in the course of the MD simulations reported below, showed that the effective charge of the penetrable
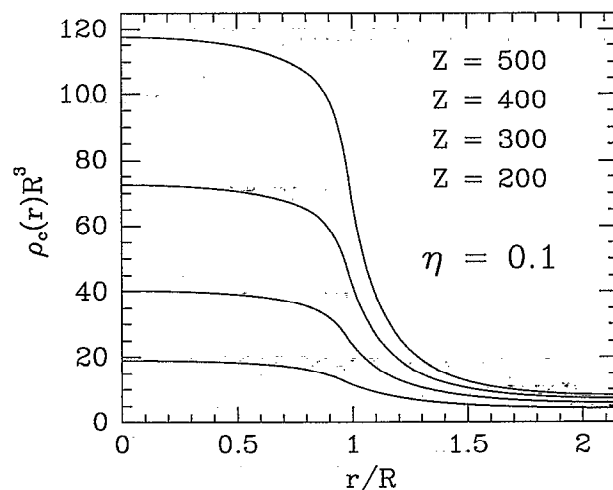

FIG. 1. Counterion density profiles $\rho_c(r)R^3$ for one macroion with charge Z in its spherical Wigner–Seitz cell. The macroion packing fraction is $\eta = 0.1$. The macroion surface is located at $r/R = 1$. The parameters are $R = 53$ nm, $T = 300$ K, $\epsilon = 78$, and $Z = 500$, 400, 300, and 200, the higher Z corresponding to the upper curve.

macroions stays very close to the physical charge Ze, relative derivations being systematically less than 1%.

Figure 1 shows typical density profiles $\rho_c(r)$ in a spherical Wigner–Seitz cell; the stabilization mechanism associated with $f_{cut}(\rho_c)$ is seen to lead to a nearly constant counterion charge inside the macroion core. As expected, the steepness of the counterion density near $r=R$ increases rapidly with increasing macroion charge Ze. The macroion charge increment Z^* is plotted in Fig. 2 vs the physical charge Z for various packing fractions η; Z^* is seen to increase nonlinearity with Z.
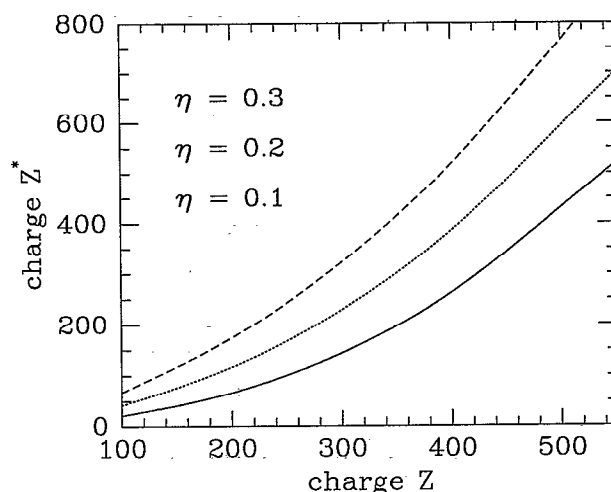

FIG. 2. Self-consistently determined counterion inside excess charge Z^* vs bare macroion charge Z for three different macroion packing fractions $\eta = 0.3$ (dashed), $\eta = 0.2$ (dotted), and $\eta = 0.1$ (solid line). The other parameters are the same as in Fig. 1.

TABLE I. Parameters for the three different runs A, B, and C. Bare charge Z, macroion packing fraction η, number of macroions N_m, additional charge Z^*, and cut-off density ρ_c^{cut} from the pseudopotential construction, as well as the data for the screened Coulomb reference pairwise potentials—the effective charge $Z_{eff}^{(i)}$ for model (i) ($i=a,b,c$) and the corresponding Debye screening parameter $\kappa_D^{(i)} R$ ($\kappa_D^{(1)} \equiv \kappa_D^{(2)}$).

Run	Z	η	N_m	Z^*	$\rho_c^{cut} R^3$	$Z_{eff}^{(a)}$	$Z_{eff}^{(b)}$	$Z_{eff}^{(c)}$	$\kappa_D^{(1)} R$	$\kappa_D^{(3)} R$
A	200	0.1	31	66.6	11.6	259	296	194	0.90	0.88
B	100	0.3	53	67.3	12.5	142	189	97.8	1.10	1.09
C	300	0.08	16	126.3	21.2	404	462	284	0.98	0.96

VIII. PRACTICAL IMPLEMENTATION

Many of the practical aspects of the present *ab initio* simulations are similar to methods developed for Car–Parrinello codes simulating ion–electron systems[13] and for the Thomas–Fermi version of such calculations.[24] This paragraph reports some technical details and parameter values of our simulations.

The "fake" mass associated with the counterion density was chosen to be $m_f = 8 \times 10^{-14} R^5 M$; this value ensured that the mean kinetic energy K_m of the macroions exceeds the fake kinetic energy K_f of the counterion degrees of freedom by a factor of 10–100. The dynamics of the macroions were implemented with a Nosé thermostat,[25] such that averages taken along the phase space trajectories are equivalent to canonical ensemble averages at an imposed temperature T; no such thermostat was used for the fake counterion degrees of freedom, which were thus governed by the usual microcanonical dynamics. Taking as time unit $\tau_0 = (MR^2/k_B T)^{1/2}$, the time step Δt was chosen sufficiently small ($\Delta t = 10^{-3}\tau_0$) to ensure excellent conservation of the total energy of the system.

In order to avoid finite size crystallization effects, the number of macroions N_m was *not* chosen equal to $2n^3$ or $4n^3$ (with n an integer), corresponding to periodic simulation cells accomodating a body-centered-cubic (bcc) or a face-centered-cubic (fcc) lattice, whenever the objective was the simulation of a fluid state of the macroions. The results reported below were obtained for $N_m = 31$ or $N_m = 53$. The counterion density $\rho_c(\mathbf{r})$ was defined on a three-dimensional grid of $\mathcal{N}^3$ points spanning the cubic simulation cell with $\mathcal{N} = 64$. This discretization of $\mathbf{r}$ space leads to $\mathcal{N}^3$ Fourier coefficients ρ_{kc}. In order to avoid spurious effects associated with the cubic symmetry of the cell, the Fourier coefficients were set equal to zero whenever $|\mathbf{k}| > 2\pi\mathcal{N}/L$ (where L is the side length of the cubic cell).

In order to allow a direct comparison of the *ab initio* results with the predictions of the usual DLVO model for the effective interactions between macroions, we carried out standard MD simulations for a system of macroions interacting via the pairwise additive DLVO potentials (6) and (7) under identical physical conditions ($T, n_m, ...$) and for identical values of the parameters (e.g., N_m).

The starting configuration $\{\mathbf{R}_j\}$ and velocities $\{\mathbf{v}_j\}$ of the macroions in an *ab initio* simulation were taken from a well-equilibrated MD run based on the corresponding DLVO potential. For momentarily fixed macroion positions $\{\mathbf{R}_j\}$, the counterion density $\rho_c^{(0)}(\mathbf{r}, \{\mathbf{R}_j\})$ was obtained by simulated annealing. The initial guess of the density profile was chosen to be a linear superposition of profiles derived from a Wigner–Seitz cell calculation and centered on $\mathbf{R}_j$. The simulated annealing process was optimized insofar as the fake kinetic energy of the counterion degrees of freedom was set to zero when the associated fake temperature was maximal. This minimization procedure turned out to be reasonably efficient, since only a few hundred time steps were necessary to achieve $K_f/K_m \simeq 10^{-8}$. Next a backstep was performed, i.e., the macroions were moved back in time by $-\Delta t/2$ and the system was once more annealed in order to determine consistent fake starting velocities. Thereafter the usual MD algorithm was used to solve the coupled equations of motion (36) and (37) for the macroion and counterion degrees of freedom. The system was equilibrated, usually for about 3000 time steps, and thereafter statistics were gathered during 10^4 time steps each of which took between 2 and 5 s of central processing unit (CPU) time on an IBM 3090.

Runs were taken for three different thermodynamic states (runs A, B, and C). In each run, the macroion radius was chosen as $R = 53$ nm, the temperature was $T = 300$ K, and the suspending fluid was water ($\epsilon = 78$). The parameters that were varied were the macroion packing fraction η and the charge Z. The values of all characteristic parameters are listed in Table I. It is to be noted that all three states under consideration correspond to the weak screening regime ($\kappa_D R \simeq 1$) due to the absence of added salt. Runs A and B describe a macroion fluid of intermediate ($\eta = 0.1$) and high ($\eta = 0.3$) packing fraction, while run C corresponds to a crystalline bcc phase of low η and high Z; the number of macroions was taken to be 16 in the latter case such that a bcc crystal fits exactly into the simulation cell.

IX. RESULTS

For the three runs listed above, we have computed a number of static and dynamical properties associated with the macroion and counterion components of the colloidal suspension; the results have been compared systematically to the predictions of the pairwise additive DLVO model in its initial[1] or modified[8,9,17] versions.

(a) The first quantity which we have analyzed is the time dependence of the counterion density profile $\rho_c^{(0)}(\mathbf{r}, \{\mathbf{R}_i(t)\})$ and a number of statistical averages and diagnostics based on this profile. The DLVO result for ρ_c is given by Eq. (26). A typical projection of ρ_c along a one-dimensional cut through the centers of two colliding macroions is shown in Figs. 3(a)–3(c) at three instants during the collision. It is seen that the corresponding DLVO den-
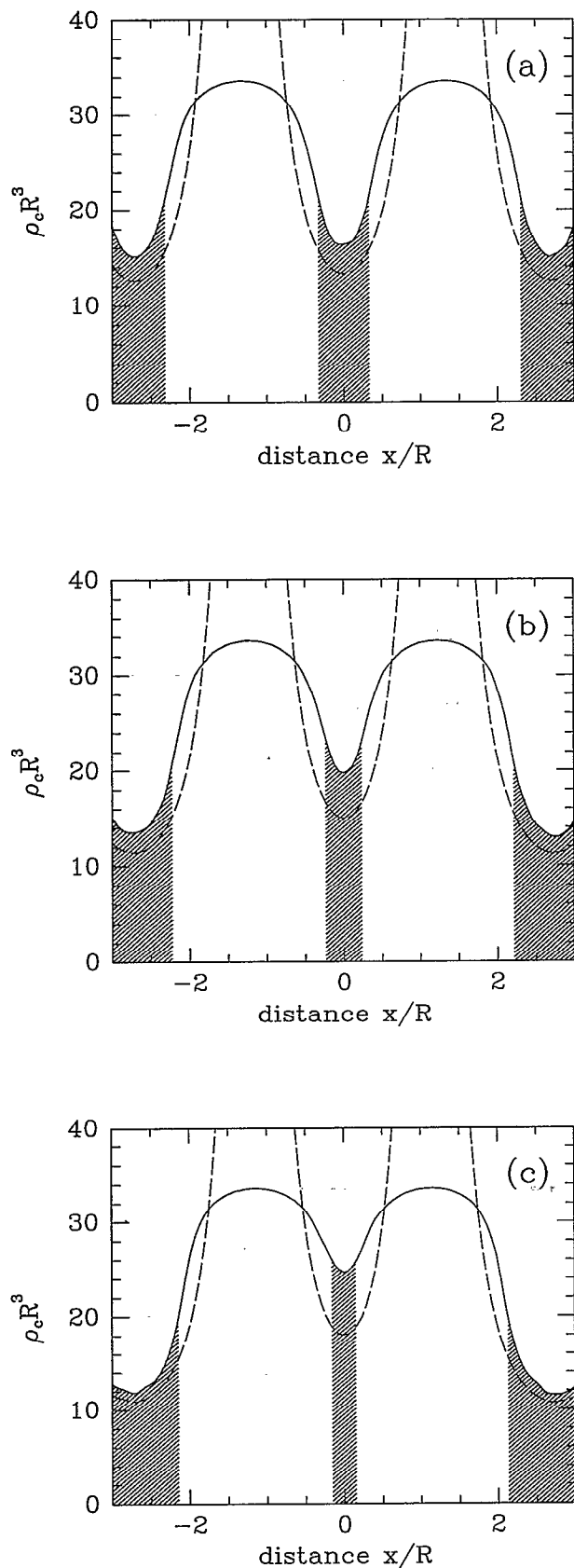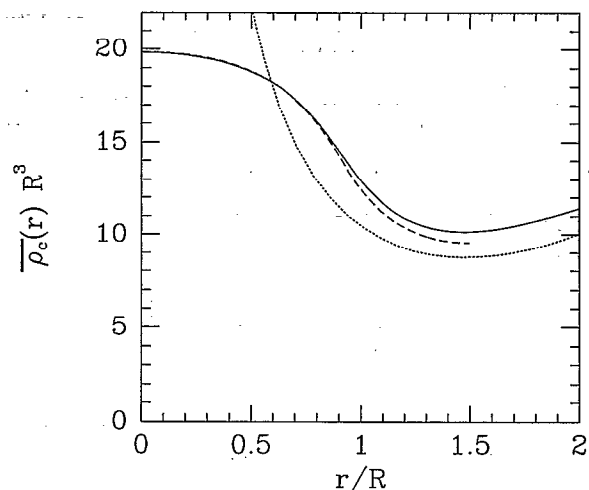
FIG. 4. Averaged counterion density profile of run B, $\bar{\rho}_c(r)R^3$ vs r/R. The density is compared with the DLVO theory (dotted line) and the corresponding result of a spherical Wigner–Seitz cell (dashed line).

sity profile, computed for the same macroion configurations, underestimates ρ_c outside the macroion cores, while the artificial counterion density inside the cores is, accordingly, too high. In particular, the mean charge inside the cores calculated from the DLVO counterion density (26) is considerably larger than $Z_{\mathrm{eff}}^{\mathrm{DLVO}}-Z$, thus illustrating the inconsistency of the DLVO approximation at high macroion concentration. The *ab initio* profiles plotted in Fig. 3 also nicely illustrate the pseudopotential construction and the stabilization of the counterion charge density inside the macroion cores. The importance of nonlinear screening effects are also apparent, in particular, in Fig. 3(c). When two macroions come very close, the counterion density between them piles up much more strongly than predicted by linear screening (i.e., DLVO) theory.

One can also define a counterion density averaged over macroion configurations according to

$$\bar{\rho}_c(r)=\left\langle \frac{1}{N_m}\sum_{i=1}^{N_m}\frac{1}{4\pi r^2}\int_{|\mathbf{r}'-\mathbf{R}_i|=r}d^2r'\,\rho_c(\mathbf{r}',\{\mathbf{R}_j\})\right\rangle.$$
(44)

This quantity is plotted in Fig. 4 for run B, and compared to the prediction of the DLVO theory and to the density profile calculated within a spherical Wigner–Seitz cell. As already pointed out in relation to Fig. 3, the DLVO density is too high inside and too low outside the macroion cores. The Wigner–Seitz profile, on the other hand, agrees rather closely with the *ab initio* result, thus justifying *a posteriori* the portability of the pseudopotential parameters. In principle, $\bar{\rho}_c(r)$ is also measurable, e.g., by small angle x-ray diffraction.[26]

Similarly one can define the mean counterion charge inside the macroion cores

$$\bar{Z}=\left\langle\frac{1}{N_m}\sum_{i=1}^{N_m}\int_{|\mathbf{r}'-\mathbf{R}_i|<R}d\mathbf{r}'\,\rho_c(\mathbf{r}',\{\mathbf{R}_j\})\right\rangle$$
(45)

and the corresponding relative fluctuation

FIG. 3. One-dimensional cut of the counterion density $\rho_c R^3$ through the center of two colliding macroions during the collision. The hatched part is the physical density outside the hard cores. The dashed line is the DLVO result for the same macroion configuration. The time interval among (a), (b), and (c) is $0.1\tau_0$. The parameters are $Z=150$, $R=53$ nm, $T=300$ K, $\epsilon=78$, and $\eta=0.3$.

TABLE II. Average inside charges $\bar{Z}$ and charges in a spherical layer around the macroions ($R < r < 1.2R$), $\bar{Z}'$, and their relative variances as defined in the text for run A and run B. AI means *ab initio* and the other pairwise potential models (a), (b), and (c) are also defined in the text.

Run	Model	$\bar{Z}$	δ_Z	$\bar{Z}'$	δ'_Z
A	AI	66.6	0.005	29.0	0.024
A	(a)	63.6	0.011	24.0	0.035
A	(b)	73.8	0.005	27.5	0.029
A	(c)	47.2	0.010	18.1	0.037
B	AI	67.7	0.005	35.7	0.044
B	(a)	60.4	0.020	27.6	0.045
B	(b)	80.1	0.020	36.3	0.048
B	(c)	42.0	0.016	19.3	0.044

$$\delta_Z = \frac{1}{\bar{Z}}\left[\left\langle \frac{1}{N_m}\sum_{i=1}^{N_m}\int_{|\mathbf{r}'-\mathbf{R}_i|<R} d\mathbf{r}'[\rho_c(\mathbf{r}',\{\mathbf{R}_j\})-\bar{Z}]^2\right\rangle\right]^{1/2}.$$
(46)

Results for $\bar{Z}$ and δ_Z are listed in Table II and compared to the values $\bar{Z}'$ and δ'_Z obtained when the integration domain is $R < |\mathbf{r}'-\mathbf{R}_i| < 1.2R$ in Eqs. (45) and (46), well beyond the Stern layer. $\bar{Z}$ is seen to deviate from Z^* by less than 1% confirming once more the validity of our pseudopotential approach. The fluctuation δ_Z turns out to be considerably smaller than its DLVO counterpart, while δ'_Z are of comparable magnitude. Furthermore, as already noted earlier, the mean DLVO charge $\bar{Z}$ is significantly larger than $Z_{\mathrm{eff}}^{\mathrm{DLVO}} - Z$, thus confirming the inconsistency of the DLVO theory due to overlap of screened Coulomb orbitals in the superposition (26).

Another "diagnostic" is provided by the fluctuation $\delta_d(r)$ of the instantaneous electric dipole $\mathbf{d}_i(r)$ associated with a spherical shell of radius r centered on the macroion position $\mathbf{R}_i$, namely,

$$\mathbf{d}_i(r) = \int_{|\mathbf{r}'-\mathbf{R}_i|=r} d^2r'\mathbf{r}'\rho_c(r',\{\mathbf{R}_j\})$$
(47)

and

$$\delta_d = \left[\left\langle \frac{1}{N_m}\sum_{i=1}^{N_m}|\mathbf{d}_i(r)|^2\right\rangle\right]^{1/2}.$$
(48)

The latter quantity is plotted in Fig. 5 together with its DLVO counterpart, which is seen to overestimate dipole fluctuations inside the macroion core, while underestimating these fluctuations for $r \gtrsim R$.

(b) An important measurable quantity which characterizes the spatial structure of the macroion component is the macroion–macroion pair distribution function $g_{mm}(r)$. The *ab initio* results from runs A and B are compared to the data obtained from standard MD simulations based on the pairwise additive, screened-Coulomb interaction model (6) in Figs. 6(a) and 6(b). Three choices have been made for the effective macroion charge Z_{eff}—the standard DLVO value (7) [model (a)], the effective charge derived from the MSA closure for both macroions and counterions[6,8,9] [model (b)], and the value proposed by Alexander *et al.*[17] on the basis of a Wigner–Seitz cell calculation [model (c)]. In the latter model, the Debye screening
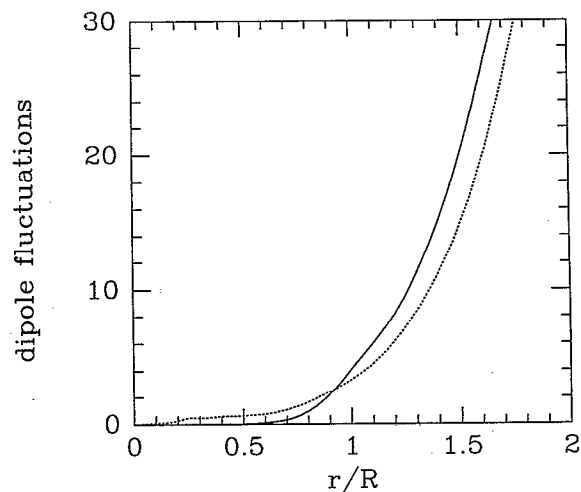

FIG. 5. Dimensionless dipole fluctuations δ_d for run B, as defined in the text, vs reduced distance for *ab initio* (full line) and DLVO (dotted line) calculations.

length is also a bit different from its DLVO value. For run A, which corresponds to a fairly low macroion packing fraction ($\eta = 0.1$), standard DLVO theory [model (a)] is seen to do surprisingly well compared to the predictions of the *ab initio* simulation, despite the significant differences between the counterion density profiles discussed previously. Model (b) (based on the MSA) strongly overestimates the macroion pair structure as anticipated in earlier work on less asymmetric, micellar systems,[8] while model (c) somewhat underestimates the correlations between macroions. The failure of model (c) is not too surprising, since in the macroion "liquid" state of relatively low packing fraction, macroions come much closer than the neighborhood of the spherical Wigner–Seitz cell boundary.

At the higher packing fraction (run B with $\eta = 0.3$), the standard DLVO theory [model (a)] is seen to break down since now it significantly underestimates the macroion pair structure. Nevertheless, it still deviates less from the *ab initio* results than models (b) and (c); the latter is found to be particularly unreliable since it leads to a considerable underestimation of macroion correlations signaling a poor choice of the effective macroion charge.

Model (b) may be improved by taking the hybrid HNC-MSA approach of Khan *et al.*[9] In this theory, the height of the first maximum of $g_{mm}(r)$ is 2.27 at $r/R = 3.65$ for the parameters of run A and 2.11 at $r/R = 2.11$ for that of run B leading to better agreement with the *ab initio* results.

The pair distribution functions in a crystalline state (run C) are shown in Fig. 6(c). Due to the small size of the simulated sample ($N_m = 16$), only the first peak of $g_{mm}(r)$ is obtained. The important observation here is that the DLVO theory [model (a)] overestimates the macroion pair structure in the solid in contrast to the opposite tendency observed in the fluid phase [Fig. 6(b)]. These opposite trends may lead to a significant shift of the macroion freezing line, as suggested by recent experiments.[15] The
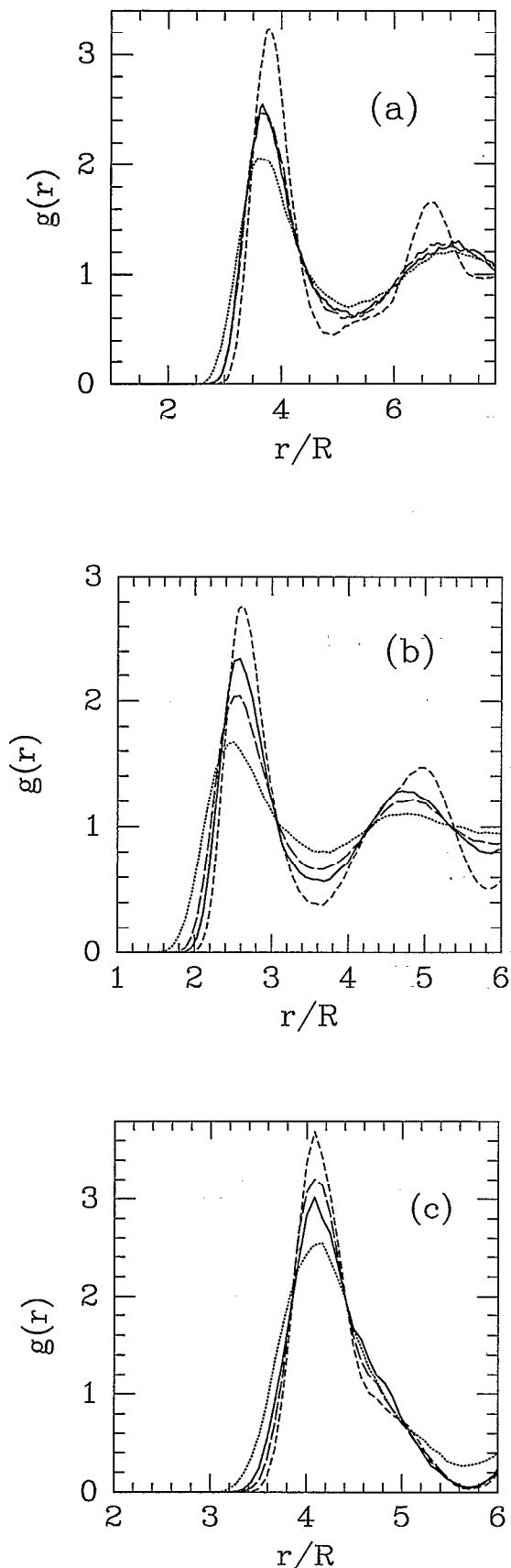
FIG. 6. Macroion–macroion pair correlation function $g_{mm}(r) \equiv g(r)$ vs reduced distance r/R for (a) run A; (b) run B; (c) run C (solid lines). The other curves are based on screened Coulomb pair potentials calculated from standard DLVO theory (a) long-dashed line; (b) short-dashed line, and (c) dotted line.
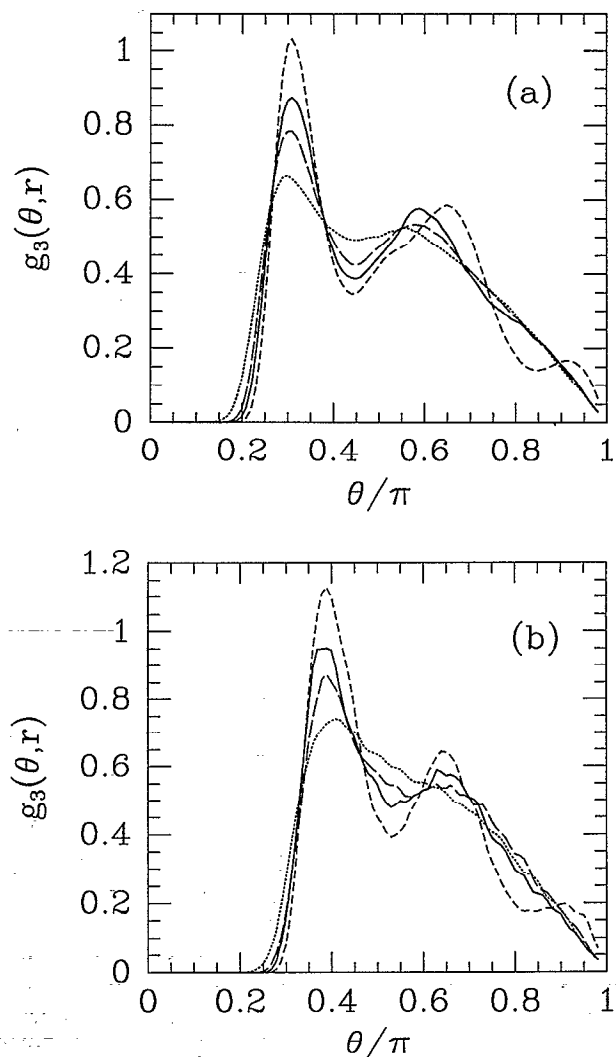

FIG. 7. Bond angle distribution function $g_3(\theta,r)$ of particle triplets that have two interparticle distances smaller than (a) $r=3.2R$; (b) $r=2.5R$ vs reduced bond angle θ/π (run B). The line types are the same as in Fig. 6. The units of $g_3(\theta,r)$ are arbitrary.

mean-square displacements of the atoms calculated from DLVO and *ab initio* simulations are comparable within statistical errors and system size limitations.

(c) Higher-order-correlation functions are more sensitive to details of the spatial distribution of particles in disordered media than the standard pair distribution functions. A convenient measure of triplet correlations is the macroion bond angle distribution function $g_3(\theta;r)$ which characterizes the distribution of bond angles θ in macroion triangles with two adjacent sides of length less than r. Examples from run B are shown in Figs. 7(a) and 7(b) for two cut-off distances ($r=2.5$ and $3.2R$). The qualitative conclusions which may be drawn from inspection of these figures confirm the observations made for the corresponding pair distribution function.

(d) The *ab initio* approach is based on **Newtonian** dynamics of the macroions as derived from the Lagrangian (35). This does not take into account the velocity-dependent interactions of the macroions with the solvent
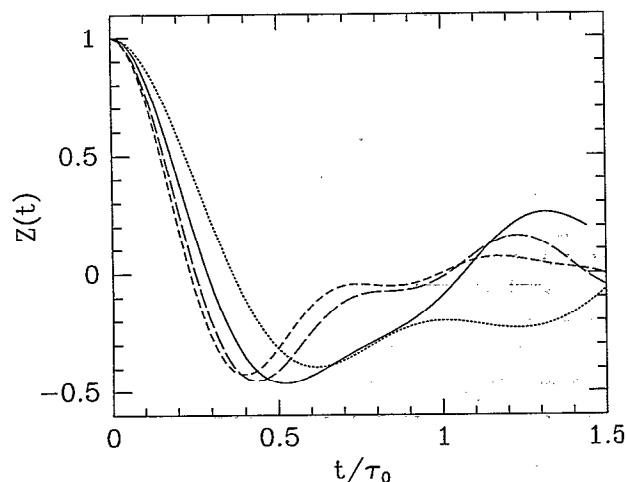
FIG. 8. Normalized macroion velocity autocorrelation function for run C (MD); $Z(t)$ vs reduced time t/τ_0; the line types are the same as in Fig. 6. This clearly shows the sensitivity of dynamical quantities to many-body forces.
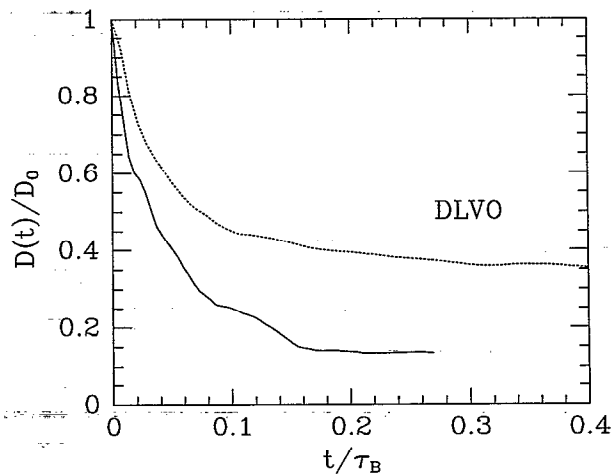

FIG. 9. Time-dependent reduced diffusion coefficient $D(t)/D_0$ vs time for the parameters of run B (Brownian dynamics): *ab initio* calculation (solid line) and the corresponding DLVO result (dotted line).

(due to friction and hydrodynamic back flow) implying irreversible **Brownian** dynamics. The static properties considered so far are independent of the nature of the dynamics, but this is, of course, not the case of time-dependent correlation functions and transport properties. Nevertheless, since dynamical properties are very sensitive to the precise form of the interactions, it is instructive to compare some results of the *ab initio* and DLVO models for time-dependent quantities. An example is shown in Fig. 8 which compares the macroion velocity autocorrelation function $Z(t)$ computed in the crystal phase (run C) by the *ab initio* MD, and by MD based on the pairwise additive screened Coulomb interactions with the three choices [(a), (b) and (c)] for Z_{eff} introduced earlier in this section. The differences in the predictions of the various models are considerable; since $Z(t)$ is a superposition of phonon modes, the comparison shows that the latter are extremely sensitive to the nature of the effective forces between macroions, and that DLVO-like models are quite incapable of reproducing correctly the *ab initio* data. The phonon density of states $g(\omega)$, which, in the harmonic approximation, is proportional to the spectral function of $Z(t)$, cannot be extracted from the data in Fig. 8 because the simulations do not extend over sufficiently long times to allow a reasonable estimate of the Fourier transforms.

(e) In order to model, at least approximately, solvent effects, we finally carried out some exploratory Brownian dynamics (BD) simulations[27] using the following algorithm for the irreversible evolution of the macroion positions:

$$\mathbf{R}_i(t+\Delta t) = \mathbf{R}_i(t) + \frac{1}{\xi} \mathbf{F}_i(t)\Delta t + (\Delta \mathbf{R})_{\text{random}}, \qquad (49)$$

where ξ is the friction coefficient which sets the Brownian time scale τ_B according to

$$\tau_B = \xi R^2/k_B T. \qquad (50)$$

ξ also determines the short-time diffusion constant of the macroions $D_0 = k_B T/\xi$. $(\Delta \mathbf{R})_{\text{random}}$ is a Gaussian-distributed random displacement of zero mean and variance

$$\overline{(\Delta \mathbf{R})^2_{\text{random}}} = 6D_0\Delta t. \qquad (51)$$

The practical implementation of BD differs somewhat from the MD procedure described earlier. Indeed, the irreversible macroion dynamics, embodied in Eq. (49), cannot be combined with the reversible fictitious dynamics of the counterion density governed by Eq. (37). Consequently, the macroions were moved according to Eq. (49) with the random displacement (51), whereas, for each macroion configuration $(\mathbf{R}_i)$, the counterion density $\rho_c[\mathbf{r}(\mathbf{R}_i)]$ was obtained by simulated annealing, starting from the profile determined at the preceding time step. While this procedure allows the use of a longer time step Δt compared to the MD case, the number of annealing steps increases with Δt so that, on balance, the BD procedure is considerably less efficient than its MD counterpart. For a given computational effort, the BD statistics are accordingly poorer. In practice, we chose $\Delta t/\tau_B = 0.002$, and $N_a = 50$ annealing steps were taken for each BD time step. Data were collected for physical parameters identical to those of run B and averages taken over 500 BD time steps. Figure 9 shows the results for the time-dependent diffusion constant

$$D(t) = \frac{1}{6t}\left\langle \frac{1}{N_m}\sum_{i=1}^{N_m}[\mathbf{R}_i(t) - \mathbf{R}_i(0)]^2\right\rangle, \qquad (52)$$

while the time dependence of the self part of the density autocorrelation function

$$F_S(k,t) = \left\langle \frac{1}{N_m}\sum_{i=1}^{N_m}\cos\{\mathbf{k}\cdot[\mathbf{R}_i(t) - \mathbf{R}_i(0)]\}\right\rangle \qquad (53)$$

is plotted in Fig. 10 for three different wave numbers $k = |\mathbf{k}|$. Comparison with the corresponding data from BD
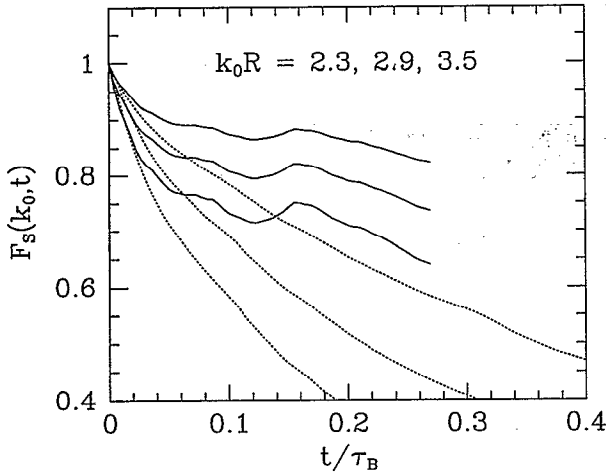
FIG. 10. The same as Fig. 9, but now for the self-part of the van Hove correlation function $F_S(k_0,t)$. $k_0 R$ is 2.3, 2.9, and 3.5; the upper curve corresponds to lower $k_0 R$.

simulations based on the pairwise additive DLVO interactions between macroions shows that diffusion, and the decay of $F_S(k,t)$, are slower when the forces between macroions are calculated from the full *ab initio* scheme, an observation which correlates well with the stronger static correlations observed in that case [cf. Fig. 6(b)]. However, in view of the limited BD statistics, the present conclusions must only be regarded as qualitative.

X. GENERALIZATION IN THE PRESENCE OF ADDED SALT

So far we have restricted ourselves to the simplest, two-component situation involving only macroions and counterions. This is an important limiting case, but, more generally, charge-stabilized suspensions also contain added salt, and hence microscopic ions that carry charges of the same sign as those of the macroions (referred to as coions), and an oppositely charged species, which plays a role similar to that of the counterions. We shall only consider the case where the two latter species are identical, so that the suspension is made up of n_m macroions per unit volume of charge Ze (which will henceforth be assumed to be positive, without loss of generality), n_+ coions of charge q_+e, and n_- counterions of charge q_-e. The electroneutrality constraint (4) now reads

$$n_m Z + n_+ q_+ + n_- q_- = 0, \tag{54}$$

while the Debye screening length (5) is generalized according to

$$\lambda_D = \frac{1}{\kappa_D} = \left[\frac{4\pi e^2}{\epsilon k_B T} (n_+ q_+^2 + n_- q_-^2) \right]^{-1/2}. \tag{55}$$

The formalism of Secs. III–VI is easily extended to treat the three-component case. The dynamical variables are now the macroion positions ($\mathbf{R}_i$) and the two density profiles $\rho_+(\mathbf{r},\{\mathbf{R}_i\})$ and $\rho_-(\mathbf{r},\{\mathbf{R}_i\})$. The various contribu-

tions to the free energy functional (10), which generalize the expressions (11)–(14), now read

$$\mathscr{F}_{\text{id}} = k_B T \sum_{\alpha = +,-} \int d\mathbf{r} \rho_\alpha(\mathbf{r}) [\ln(\Lambda_c^3 \rho_\alpha(\mathbf{r})) - 1], \tag{56}$$

$$\mathscr{F}_{\text{ext}} = \sum_{\alpha = +,-} \int d\mathbf{r} \, \rho_\alpha(\mathbf{r}) V_{\text{ext}}^{(\alpha)}(\mathbf{r},\{\mathbf{R}_j\})$$

$$= \sum_{\alpha = +,-} \sum_{j=1}^{N_m} \int d\mathbf{r} \, \rho_\alpha(\mathbf{r}) v_{m\alpha}(|\mathbf{r} - \mathbf{R}_j|), \tag{57}$$

$$\mathscr{F}_{cc} = \frac{e^2}{2\epsilon} \int \int d\mathbf{r} \, d\mathbf{r}' \frac{\rho_Q(\mathbf{r})\rho_Q(\mathbf{r}')}{|\mathbf{r} - \mathbf{r}'|}, \tag{58}$$

where $\rho_Q(\mathbf{r}) = q_+\rho_+(\mathbf{r}) + q_-\rho_-(\mathbf{r})$ denote the local charge density of the microscopic ions (coions and counterions).

For the correlation part of the free energy functional $\mathscr{F}[\rho_+(\mathbf{r}), \rho_-(\mathbf{r})]$, we adopt once more the LDA

$$\mathscr{F}_{\text{corr}} = k_B T \int d\mathbf{r} \, \rho_N(\mathbf{r}) \Psi^{\text{exc}}[T, \rho_+(\mathbf{r}), \rho_-(\mathbf{r})], \tag{59}$$

where $\rho_N(\mathbf{r}) = \rho_+(\mathbf{r}) + \rho_-(\mathbf{r})$ denotes the local number density of microscopic ions, while Ψ^{exc} is the reduced excess free energy of a homogeneous fluid of coions and counterions with densities $\rho_+ = \rho_+(\mathbf{r})$ and $\rho_- = \rho_-(\mathbf{r})$ immersed in a uniform, positive neutralizing background of density $\rho_Q = -\rho_Q(\mathbf{r})$, which compensates for the excess of negative counterion over positive coion charge. Due to the Coulomb attraction between coions and counterions, this model is stable only for finite size ions. If the latter are taken to be spheres of diameter σ, the required excess free energy Ψ^{exc} may be calculated from the analytic solution of the MSA for this model.[28] For sufficiently weak Coulomb coupling $J = e^2/(\epsilon k_B T \sigma)$, the MSA result goes over into the Debye–Hückel limit for the excess free energy per ion $\Psi_{\text{DH}}^{\text{exc}} = F_{\text{DH}}^{\text{exc}}/(N k_B T)$, namely

$$\Psi_{\text{DH}}^{\text{exc}}(T, \rho_+, \rho_-) = -\frac{1}{4\pi n^*} \left[\ln(1 + \kappa^*) - \kappa^* + \frac{1}{2}\kappa^{*2} \right]$$

$$+ \frac{4\pi n_Q^{*2} J}{3n^* \kappa^{*2}} \left[\ln(1 + \kappa^*) - \kappa^* - \frac{1}{4}\kappa^{*2} \right], \tag{60}$$

where $n^* = (\rho_+ + \rho_-)\sigma^3$, $n_Q^* = (q_+\rho_+ + q_-\rho_-)\sigma^3$, and $\kappa^* = \kappa_D \sigma$. This form of the free energy of the homogeneous fluid of microscopic ions in a uniform neutralizing background should be sufficiently accurate, except at high concentrations of added salt.

The *ab initio* scheme then follows along the lines described in Sec. VI. The Lagrangian (35) now contains two fictitious kinetic energy terms associated with the two density profiles $\rho_+(\mathbf{r})$ and $\rho_-(\mathbf{r})$, and the equation of motion (37) for the counterion density must be replaced by two similar equations governing the evolution of $\rho_+(\mathbf{r})$ and $\rho_-(\mathbf{r})$. The practical implementation described in Secs. VII and VIII carries over to the present case. Since the macroions repel the coions, the local density $\rho_+(\mathbf{r},\{\mathbf{R}_i\})$ decreases smoothly in the vicinity of the macroion surfaces

($|\mathbf{r}-\mathbf{R}_i| \simeq R$), so that there is no need for a pseudopotential construction similar to that used for the counterions which are strongly attracted by the macroions.

XI. DISCUSSION AND OUTLOOK

In summary, we have proposed and implemented an *ab initio* procedure for the simulation of charge-stabilized colloidal suspensions, which combines Molecular (or Brownian) Dynamics for the macroions with a density functional description of the microscopic counterions and coions within an adiabatic framework inspired directly from the Car–Parrinello method[12,13] developed for quantum-mechanical ion–electron systems. More precisely, the present scheme may be looked upon as the classical counterpart of a recent, approximate version of the Car–Parrinello method, which only considers the electron density profile within the LDA (i.e., the nonlinear Thomas–Fermi approximation) rather than focussing on the one-electron Kohn–Sham orbitals.[24] Apart from the use of the LDA in the calculation of rather small correlational contribution to the free energy functional (10), the present scheme may be regarded as essentially "exact", at least as regards the calculation of static properties of the "primitive model" for colloidal suspensions. The model does, of course, neglect the discrete nature of the suspending fluid (generally water), but apart from hydration effects in the vicinity of the macroion surfaces, the continuum picture should not have a significant effect on the density profiles and hence on the effective interactions between macroions.

We are able to overcome the technical difficulties associated with the piling up of counterions at the oppositely charged macroion surfaces, as reflected in a sharp rise of $\rho_c(\mathbf{r},\{\mathbf{R}_i\})$ near $|\mathbf{r}-\mathbf{R}_i| \simeq R$, by introducing a classical pseudopotential scheme, which is reminiscent of ion–electron pseudopotentials in metallic and covalent systems.

Although our *ab initio* procedure can easily cope with the physically important situation of added salt, as shown in the last section, the numerical implementations presented in this paper deal only with the simplest case of a fully dialized suspension, which only contains macroions and counterions. We have compared systematically the predictions of our *ab initio* procedure, which properly includes nonlinear screening and many-body forces between macroions based on the pairwise additive DLVO model and two of its variants. The main conclusion is that standard DLVO theory [with the effective macroion charge (7)] yields a reasonably accurate description of the macroion pair structure, at least at intermediate packing fraction. At higher packing fractions, the DLVO theory underestimates this pair structure, but does better than the modified versions which use different values of the effective macroion charge. The apparant success of the DLVO theory may be partially fortuitous since the predicted counterion density profile differ substantially from those obtained by the *ab initio* procedure. Moreover, it must be stressed that the salt-free states explored in this work belong to the weak screening regime since $\kappa_D R \simeq 1$. We expect that in the presence of a high concentration of

added salt, i.e., in the strong screening regime $\kappa_D R \gg 1$, nonlinear effects will be considerably enhanced, so that the discrepancies between *ab initio* and DLVO simulations will become much larger. Simulations in this regime are at present being planned. Other extensions which are being considered involve low-dimensional colloidal systems including clays[29] and colloidal monolayers confined between parallel glass plates.[30]

Finally, the present density functional formulation provides a natural framework for a systematic derivation of effective pair and many-body interactions between macroions. More work along these lines is in progress.

APPENDIX A: EFFECTIVE HAMILTONIAN FOR THE MACROIONS

In this appendix, it is shown how the effective Hamiltonian (9) may be derived from the primitive model Hamiltonian (8) within the adiabatic approximation, which is fully justified in view of the enormous difference in time scales associated with the macroions and counterions. To this purpose, the Boltzmann factor of the Hamiltonian (8) is integrated over counterionic degrees of freedom

$$[\exp(-\beta H)]_c \equiv \int d^N\mathbf{r}\, d^N\mathbf{p}\, \exp(-\beta H)$$

$$= \exp[-\beta(K_m + V_{mm})]$$

$$\times [\exp\{-\beta(K_c + V_{mc} + V_{cc})\}]_c \quad (61)$$

with $\beta \equiv 1/k_B T$. The effective macroion Hamiltonian is then defined by

$$H_{\text{eff}} = -k_B T \ln[\exp(-\beta H)]_c$$

$$= K_m + V_{mm}$$

$$-k_B T \ln[\exp\{-\beta(K_c + V_{mc} + V_{cc})\}]_c. \quad (62)$$

For a given macroion configuration $\{\mathbf{R}_i\}$, the counterions form an inhomogeneous plasma of point charges $-qe$, in the "external" field due to the macroions. The corresponding exact one-particle density will be denoted by $\rho_c(\mathbf{r},\{\mathbf{R}_i\})$.

Consider an auxiliary continuous (i.e., structureless), inhomogeneous background of charge density $qe\rho(\mathbf{r}) \equiv qe\rho_c(\mathbf{r},\{\mathbf{R}_i\})$. Its self energy is

$$V_{bb} = \frac{q^2 e^2}{2\epsilon} \int\int d\mathbf{r}\, d\mathbf{r}' \frac{\rho(\mathbf{r})\rho(\mathbf{r}')}{|\mathbf{r}-\mathbf{r}'|}, \quad (63)$$

while the counterion-background interaction energy is

$$V_{bc} = -\frac{q^2 e^2}{\epsilon} \sum_{i=1}^{N_c} \int d\mathbf{r} \, \frac{\rho(\mathbf{r})}{|\mathbf{r} - \mathbf{r}_i'|} . \tag{64}$$

Now add and subtract $V_{bb} + V_{bc}$ from the exponent of the Boltzmann factor in Eq. (62). Noting that V_{bb} is independent of counterion coordinates, Eq. (62) may finally be rewritten as

$$H_{\text{eff}} = K_m + V_{mm} - V_{bb}$$
$$- k_B T \ln[\exp\{-\beta(K_c + V_{cc} + V_{bb} + V_{bc})\}$$
$$\times \exp\{-\beta(V_{mc} - V_{bc})\}]_c . \tag{65}$$

The argument of the first exponential on the right-hand side of Eq. (65) is exactly the Hamiltonian of a "one-component plasma" (OCP) in an inhomogeneous background of density $\rho(\mathbf{r})$; this Hamiltonian will be denoted by $H_0[\rho_c(\mathbf{r})]$ and the corresponding partition function by $Q_0[\rho(\mathbf{r})]$. With these notations, Eq. (65) may be rewritten in the form

$$H_{\text{eff}} = K_m + V_{mm} - V_{bb}$$
$$- k_B T \ln\{Q_0[\rho(\mathbf{r})]\langle \exp\{-\beta(V_{mc} - V_{bc})\}\rangle_0\}, \tag{66}$$

where $\langle \cdots \rangle_0$ denotes a canonical average weighted by the OCP Hamiltonian $H_0[\rho(\mathbf{r})]$. We have thus derived the exact result

$$H_{\text{eff}} = K_m + V_{mm} - V_{bb} + \mathscr{F}_0[\rho(\mathbf{r})]$$
$$- k_B T \ln\langle \exp\{-\beta(V_{mc} - V_{bc})\}\rangle_0, \tag{67}$$

where $\mathscr{F}_0$ is the free energy of the inhomogeneous OCP. Noting that $V_{mc} - V_{bc}$ may be expected to have only small fluctuations, it is reasonable to replace the last term in Eq. (67) by the first-order cumulant, i.e.,

$$- k_B T \ln\langle \exp\{-\beta(V_{mc} - V_{bc})\}\rangle_0$$
$$\simeq \langle V_{mc} - V_{bc}\rangle_0$$
$$= \sum_{i=1}^{N_m} \int d\mathbf{r} \, \rho(\mathbf{r}) v_{mc}(|\mathbf{r} - \mathbf{R}_i|)$$
$$+ \frac{q^2 e^2}{\epsilon} \iint d\mathbf{r} \, d\mathbf{r}' \, \frac{\rho(\mathbf{r})\rho(\mathbf{r}')}{|\mathbf{r} - \mathbf{r}'|} . \tag{68}$$

Substituting Eq. (68) into Eq. (67), remembering Eq. (63), and separating $\mathscr{F}_0[\rho(\mathbf{r})]$ into ideal and correlation contributions, we finally arrive at the desired result

$$H_{\text{eff}} = K_m + V_{mm} + V_{bb} + \mathscr{F}_{\text{id}}[\rho(\mathbf{r})] + \mathscr{F}_{\text{corr}}[\rho(\mathbf{r})]$$
$$+ \mathscr{F}_{\text{ext}}[\rho(\mathbf{r})] \tag{69}$$

which coincides with the result summarized in Eqs. (9) and (10), since V_{bb} is identical with the Coulomb contribution $\mathscr{F}_{cc}$ [Eq. (13)] to the free energy functional.

[1] E. J. W. Verwey and J. T. G. Overbeek, *Theory of the Stability of Lyophobic Colloids* (Elsevier, Amsterdam, 1948).
[2] For a recent review, see P. N. Pusey, in *Liquids, Freezing and the Glass Transition*, edited by J. P. Hansen, D. Levesque, and J. Zinn-Justin (North-Holland, Amsterdam, 1991).
[3] See, e.g., E. Y. Shen, C. F. Wu, S. H. Chen, and L. Blum, Phys. Rev. A 32, 3807 (1985); W. Härtl and H. Versmold, J. Chem. Phys. 88, 7157 (1988).
[4] See, e.g., J. P. Hansen and I. R. McDonald, *Theory of Simple Liquids*, 2nd ed. (Academic, London, 1986).
[5] M. P. Allen and D. J. Tildesley, *Computer Simulation of Liquids* (Clarendon, Oxford, 1989).
[6] M. Medina-Noyola and D. A. McQuarrie, J. Chem. Phys. 73, 6279 (1980).
[7] G. Senatore and L. Blum, J. Phys. Chem. 89, 2676 (1985).
[8] L. Belloni, J. Chem. Phys. 85, 519 (1986).
[9] S. Khan, T. L. Morton, and D. Ronis, Phys. Rev. A 35, 4295 (1987).
[10] L. Belloni, J. Chem. Phys. 88, 5143 (1988).
[11] P. Linse, J. Chem. Phys. 93, 1376 (1990); 94, 3877 (1991); 94, 8227 (1991).
[12] R. Car and M. Parrinello, Phys. Rev. Lett. 55, 2471 (1985).
[13] For a recent review of the Car–Parrinello method, see D. K. Remler and P. A. Madden, Mol. Phys. 70, 921 (1990).
[14] H. Löwen, P. A. Madden, and J. P. Hansen, Phys. Rev. Lett. 68, 1081 (1992).
[15] E. B. Sirota, H. D. Ou-Yang, S. K. Sinha, P. M. Chaikin, J. D. Axe, and Y. Fuji, Phys. Rev. Lett. 62, 1524 (1989).
[16] D. Bratko, H. L. Friedman, and E. C. Zhong, J. Chem. Phys. 85, 377 (1986).
[17] S. Alexander, P. M. Chaikin, P. Grant, G. J. Morales, P. Pincus, and D. Hone, J. Chem. Phys. 80, 5776 (1984).
[18] R. Evans, in *Liquids at Interfaces*, edited by J. Charvolin, J. F. Joanny, and J. Zinn-Justin (North-Holland, Amsterdam, 1990).
[19] M. J. Stevens and M. O. Robbins, Europhys. Lett. 12, 81 (1990).
[20] Also the Onsager-"charge smearing" has some relation to a density functional description of counterions; see e.g., Y. Rosenfeld, Phys. Rev. A 26, 3622 (1982); Y. Rosenfeld, D. Levesque, and J. J. Weis, ibid. 39, 3079 (1989).
[21] The OCP is, with the Ising model and the hard sphere system, one of the most widely studied models in statistical mechanics. For reviews, see, e.g., M. Baus and J. P. Hansen, Phys. Rep. 59, 1 (1980), or S. Ichimaru, H. Iyetomi, and S. Tanaka, ibid. 149, 91 (1987).
[22] R. Abe, Prog. Theor. Phys. 22, 213 (1959).
[23] J. P. Hansen, in *Molecular Dynamics Simulation of Statistical Mechanical Systems*, edited by G. Ciccotti and W. G. Hoover (North-Holland, Amsterdam, 1986).
[24] J. Clérouin, G. Zérah, D. Benisti, and J. P. Hansen, Europhys. Lett. 13, 685 (1990); G. Zérah, J. Clérouin, and E. L. Pollock, Phys. Rev. Lett. 69, 446 (1992).
[25] S. Nosé, Mol. Phys. 52, 255 (1984).
[26] C. F. Wu, S. H. Chen, L. B. Shih, and J. S. Lin, Phys. Rev. Lett. 61, 645 (1988).
[27] D. L. Ermak, J. Chem. Phys. 62, 4189 (1975); 62, 4197 (1975).
[28] M. Parrinello and M. Tosi, Chem. Phys. Lett. 64, 579 (1979).
[29] I. S. Sogami, T. Shinohara, and M. V. Smalley, Mol. Phys. 74, 599 (1991).
[30] C. A. Murray, W. O. Sprenger, and R. A. Wenk, J. Phys. Condensed Matter 2, SA 385 (1990) and references therein.